

# Carbyne from first principles: Chain of C atoms, a nanorod or a nanorope?

Mingjie Liu,<sup>1</sup> Vasilii I. Artyukhov,<sup>1</sup> Hoonkyung Lee,<sup>1,\*</sup> Fangbo Xu,<sup>1</sup> and Boris I. Yakobson<sup>1,2,3,#</sup>

<sup>1</sup>Department of Mechanical Engineering and Materials Science, <sup>2</sup>Department of Chemistry, and <sup>3</sup>Smalley Institute for Nanoscale Science and Technology, Rice University, Houston, Texas 77005, USA

\* Present address: Department of Physics, Konkuk University, Seoul, 143-701, Korea

# e-mail: biy@rice.edu

We report an extensive study of the properties of carbyne using first-principles calculations. We investigate carbyne's mechanical response to tension, bending, and torsion deformations. Under tension, carbyne is about twice as stiff as the stiffest known materials and has an unrivaled specific strength of up to  $7.5 \times 10^7$  N·m/kg, requiring a force of  $\sim 10$  nN to break a single atomic chain. Carbyne has a fairly large room-temperature persistence length of about 14 nm. Surprisingly, the torsional stiffness of carbyne can be zero but can be 'switched on' by appropriate functional groups at the ends. We reconstruct the equivalent continuum-elasticity representation, providing the full set of elastic moduli for carbyne, showing its extreme mechanical performance (*e.g.* a Young's modulus of 32.7 TPa with an effective mechanical thickness of 0.772 Å). We also find an interesting coupling between strain and band gap of carbyne, which is strongly increased under tension, from 3.2 to 4.4 eV under a 10% strain. Finally, we study the performance of carbyne as a nanoscale electrical cable, and estimate its chemical stability against self-aggregation, finding an activation barrier of 0.6 eV for the carbyne–carbyne cross-linking reaction and an equilibrium cross-link density for two parallel carbyne chains of 1 cross-link per 17 C atoms (2.2 nm).

## Introduction

Carbon exists in the form of many allotropes: zero-dimensional  $sp^2$  fullerenes,<sup>1</sup> the two-dimensional  $sp^2$  honeycomb lattice of graphene<sup>2</sup> (parent to graphite and carbon nanotubes), or three-dimensional  $sp^3$  crystals—diamond and lonsdaleite. Each allotrope has notably different electronic and mechanical properties. For instance, graphene has the characteristic semimetal electronic structure with a linear band dispersion<sup>3</sup> and an extraordinarily high electron mobility.<sup>4</sup> In contrast, diamond is a wide-band-gap insulator and one of the hardest natural materials known.

Carbon can also exist in the form of carbyne, an infinite chain of  $sp$ -hybridized carbon atoms. It has been theoretically predicted that carbyne may be stable at high temperatures ( $\sim 3000$  K).<sup>5</sup> Indications of naturally-formed carbyne were observed in such environments as shock-compressed graphite, interstellar dust, and meteorites.<sup>6–8</sup> The carbyne-ring structure is the ground state for small (up to about 20 atoms) carbon clusters.<sup>9</sup> Experimentally, many different methods of fabrication of

finite-length carbon chains have been demonstrated, including gas-phase deposition, epitaxial growth, electrochemical synthesis, or ‘pulling’ the atomic chains from graphene or carbon nanotubes.<sup>10–17</sup> Recently, chains with length of up to 44 atoms have been chemically synthesized in solution.<sup>18</sup> Many interesting physical applications of carbynes have been proposed theoretically, including nanoelectronic/spintronic devices,<sup>19–23</sup> and hydrogen storage.<sup>24</sup> Moreover, very recently, such complex molecular mechanisms as rotaxanes based on carbyne chains have been synthesized.<sup>25,26</sup> All of these advances make the understanding of mechanical behavior of carbyne more and more important.<sup>27</sup>

Albeit there exists a considerable body of literature on the structure<sup>28,29</sup> and mechanics<sup>30–33</sup> of carbyne, it is very scattered and has thus failed so far to provide a well-rounded perspective. Here we address this shortage and put forward a coherent picture of carbyne mechanics and its interplay with chemical and electronic phenomena.

## Results and discussion

We begin by discussing the structure of carbyne. One textbook structure of one-dimensional chain of C atoms is the cumulene ( $=C=C=$ ), known to undergo a Peierls transition<sup>34</sup> into the polyne ( $-C\equiv C-$ ) form. Our calculations confirm this instability, showing an energy difference of 2 meV per atom in favor of the polyne structure. The calculated cohesive energy of polyne is  $E_c = 6.99$  eV per atom.

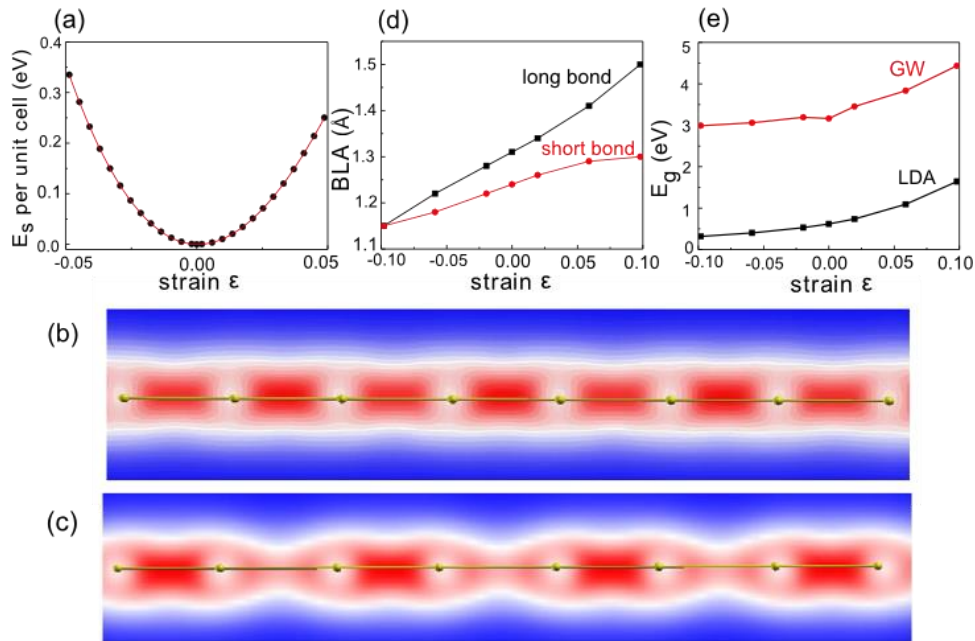


**Figure 1: Carbyne under tension.** (a) DFT calculations of energy as a function of strain  $\epsilon$ . The electronic density of carbyne (polyne) (b) in equilibrium and (c) under tension shows a more pronounced bond alternation in strained carbyne. (d) Bond length alternation and (e) band gap increase as a function of strain.

**Carbyne under tension: the strongest nanowire.** The most basic mechanical property of the carbyne chain is its tensile stiffness, defined as

$$C = \frac{1}{a} \frac{\partial^2 E}{\partial \varepsilon^2}, \quad (1)$$

where  $a$  is the unit cell length (2.565 Å),  $E$  is the strain energy per two C atoms, and  $\varepsilon$  is the strain. Fitting 1 to the data with a fourth-order polynomial (**Fig. 1 (a)**) yields a tensile stiffness of  $C = 95.56 \text{ eV/Å}$ . A more informative measure from the engineering standpoint is the specific stiffness of the material, which for carbyne works out to be  $\sim 10^9 \text{ N}\cdot\text{m/kg}$ . This is a more than twofold improvement over the two stiffest known materials—carbon nanotubes and graphene ( $4.5 \times 10^8 \text{ N}\cdot\text{m/kg}^{35-37}$ )—and almost threefold, over diamond ( $3.5 \times 10^8 \text{ N}\cdot\text{m/kg}^{38}$ ).

Another important metric of engineering materials is their specific strength. The tensile strength is generally difficult to predict theoretically, therefore we approach the problem from two complimentary perspectives. One method to evaluate the ideal strength of carbyne is to compute the phonon instability point—the strain at which imaginary frequencies appear in the phonon spectrum.<sup>36</sup> We found that in carbyne, this event occurs at a critical strain of 18–19%, at a pulling force of 11.66 nN. Another approach is to treat fracture as an activated bond rupture process and compute its activation barrier  $E_a(\varepsilon)$  as a function of strain.<sup>39</sup> The computed  $E_a(\varepsilon)$  dependence shows the expected decrease with tension, and at a strain of  $\sim 9\%$  (9.3 nN) it reaches a characteristic magnitude of 1 eV for which transition state theory predicts an expected lifetime on the order of  $\sim 1$  day. Thus the estimated breaking force of a carbyne chain is **9.3–11.7 nN** (this is  $>100\times$  the previous literature report of 0.9 nN,<sup>32</sup> demonstrating the inadequateness of the ReaxFF forcefield used therein for carbyne mechanics). This force translates into a specific strength of  **$6.0\text{--}7.5 \times 10^7 \text{ N}\cdot\text{m/kg}$** , again significantly outperforming every known material including graphene ( $4.7\text{--}5.5 \times 10^7 \text{ N}\cdot\text{m/kg}^{35,36}$ ), carbon nanotubes ( $4.3\text{--}5.0 \times 10^7 \text{ N}\cdot\text{m/kg}^{40,41}$ ), and diamond ( $2.5\text{--}6.5 \times 10^7 \text{ N}\cdot\text{m/kg}^{42}$ ). The details of calculations are described in Supplementary Materials.

It is interesting to see what happens to the bond length alternation (BLA) of carbyne under tension.<sup>27</sup> **Fig. 1 (b, c)** shows the electronic densities of carbyne in free-standing state and at a 10% strain. While in the first case (b), the BLA is barely noticeable in the plot, the second (c) shows very clear distinction between the ‘single’ and ‘triple’ bonds. The BLA magnitude is increased from 0.07 Å in free carbyne to 0.20 Å when  $\varepsilon = 10\%$  (**Fig. 1 (d)**). Naturally, this change in the BLA has big ramifications for the electronic properties of carbyne. **Fig. 1 (e)** shows the variation of the band gap with strain computed using the local density approximation and with a quasiparticle energy correction ( $G_0W_0$ ).<sup>43</sup> The LDA band gap width increases from 0.6 eV at 0% to  $\sim 1.6$  eV at a 10% strain. The  $GW$  correction to the band gap is about 2.6–2.8 eV, essentially independent of the strain. Large correction magnitudes are typical for low-dimensionality systems with their weak Coulomb screening, and in carbyne it is especially pronounced (compare to 1 eV in carbon nanotubes<sup>44</sup> and 2 eV in graphene nanoribbons<sup>45</sup>). Thus, the total band gap changes from 3.2 to 4.4 eV (38%) upon straining carbyne by 10%, showing carbyne’s great prospects for opto-/electromechanical applications. (An independent study reporting the same effects<sup>46</sup> came out while the present manuscript was in preparation.) The nature of this effect and its unusual consequences are explored more deeply elsewhere.<sup>23</sup>

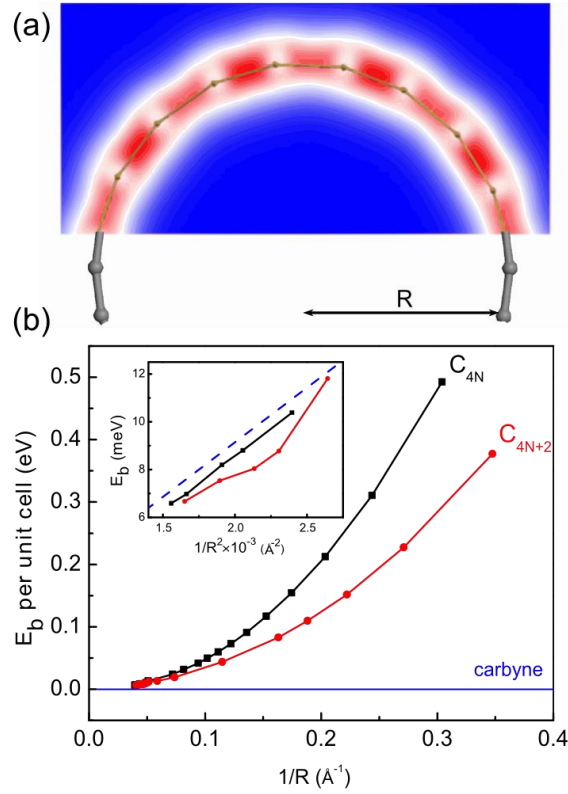


**Figure 2. Bending stiffness of carbyne.** (a) The carbon ring model with its electron density distribution, showing the usual bond alternation pattern. (b) The energy as a function of ring curvature calculations used to extract the bending modulus value.

**Bending stiffness: nanorod or nanorope?** Given the extreme tensile stiffness of carbyne, it is interesting to investigate how this material performs under bending deformations. The bending stiffness is defined as

$$K = \frac{1}{a} \frac{\partial^2 E}{\partial q^2}, \quad (2)$$

where  $a$  is again the unit cell and  $q$  is the curvature. To calculate the bending energy of carbyne, we use the model of carbon rings because of their advantage of having a constant uniform curvature defined by their radius,  $q = 1/R$  (**Fig. 2, a**). The BLA pattern is retained in the rings having an even number of atoms, as seen from the electronic density distribution in **Fig. 2 (a)**. Additional care must be taken with carbyne rings since the Jahn–Teller distortion (the counterpart of Peierls instability in non-linear molecules) is different in the  $C_{4N}$  and  $C_{4N+2}$  families of rings.<sup>47–49</sup> The  $C_{4N+2}$  rings undergo a second-order distortion which produces little/no BLA at small  $N$ . Because of this, the bending stiffness in the two families differs for small rings, but as  $N$  increases ( $q \rightarrow 0$ ), the difference gradually disappears, and the stiffness of both families approaches the common limit of infinite straight carbyne, which the extrapolation of our results places at  $K = 3.56 \text{ eV}\cdot\text{\AA}$ . A similar extrapolation of the ring energies disagrees with an explicit periodic infinite-chain calculation by only about 0.3 meV/atom, showing the robustness of our procedure.

**Persistence length.** In order to determine whether this value of  $K$  is large or small, we can further characterize the bending stiffness of carbyne using the concept of persistence length familiar from polymer physics. It is defined as  $l_p = K/k_B T$ , where

$k_B$  is the Boltzmann constant and  $T$  is the temperature. Using our value of  $K$ , the persistence length of carbyne at 300 K is roughly  $l_p = \mathbf{14\text{ nm}}$ , or about 110 C atoms. This can be compared to the persistence length of various important polymers, as presented in Table 1. As we see, carbyne is relatively stiff for a polymer and comparable to narrowest graphene nanoribbons, and it is about 13 times as stiff as a dsDNA rod (mind the 2-nm diameter of the latter).

**Table 1. Persistence length of carbyne as compared to several important polymers**

<b>Polymer</b>	<b><math>l_p</math> (nm)</b>
polyacrylonitrile <sup>50</sup>	0.4–0.6
polyacetylene <sup>51</sup>	1.3
single-stranded DNA <sup>52,53</sup>	1–4
polyaniline <sup>54</sup>	9
double-stranded DNA (dsDNA) <sup>55</sup>	45–50
graphene nanoribbons <sup>56</sup>	10–100
<b>carbyne (present work)</b>	<b>14</b>

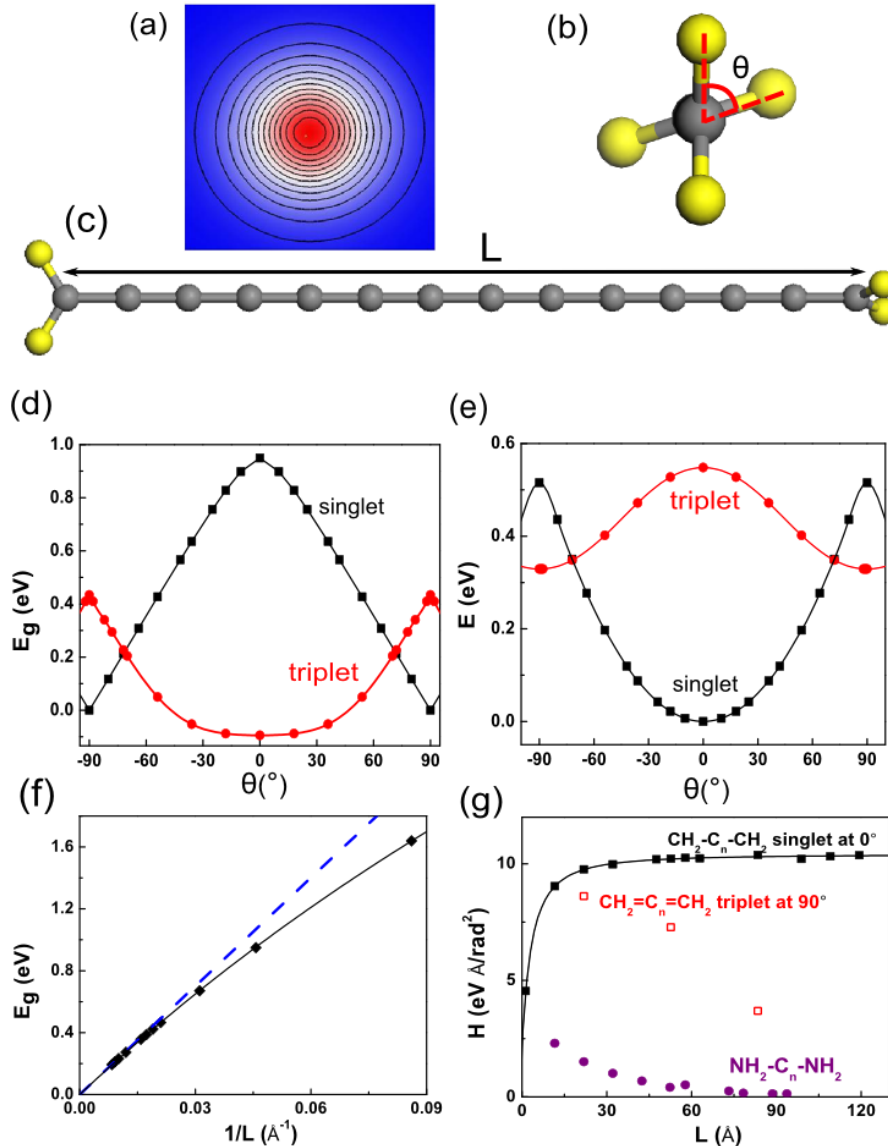


**Figure 3. End-group-induced torsional stiffness of carbyne.** (a) Cross-section of the electronic density of carbyne. (b) Front and (c) side view of a carbyne chain with attached  $=\text{CH}_2$  handles. (d) Band gap and (e) energy as a function of the torsional angle. (f) Band gap and (g) torsional stiffness dependence on the chain length. The blue line in (f) is fitted by  $E = A/L$  and black line is fitted by  $E = A/(L + L_0)$

**Carbyne under torsion: chemically modulated spring.** The torsional stiffness of a rod of length  $L$  is expressed as

$$H = L \frac{\partial^2 E}{\partial \theta^2}, \quad (3)$$

where  $\theta$  is the torsion angle. Looking at the electron density distribution along the atomic chain (**Fig. 3, a**), one immediately recognizes a problem with this definition. Because of the cylindrical symmetry of the density—and, consequently, all relevant physical observables—it is impossible to define  $\theta$ , and thus  $H$  has to be zero. However, we can solve this problem by attaching functional group ‘handles’ at the chain ends to break the cylindrical symmetry (**Fig. 3, b and c**). Further, depending on the character of the passivation— $sp^3$  or  $sp^2$ —one should expect different effects on the torsional stiffness.<sup>30</sup>

We considered different functional groups, including methyl (CH<sub>3</sub>), phenyl (C<sub>6</sub>H<sub>5</sub>), and hydroxyl (OH) as *sp*<sup>3</sup> radicals, and amine (NH<sub>2</sub>, planar) and methylene (CH<sub>2</sub>) groups from the *sp*<sup>2</sup> family. With methyl and hydroxyl, we find that the single C–R bond at the end interfaces so smoothly with the single–triple bond system of carbyne as to result in a completely free unhindered rotation. Moreover, phenyl handles also rotated freely, suggesting a single bond between the carbyne and the aromatic ring. Only the =CH<sub>2</sub> (and, weakly, NH<sub>2</sub>) termination shows a detectable torsional stiffness.

Before we present the numerical results, an interesting question to consider is how this stiffness could emerge at the electronic-structure level. Consider the behavior of band gap as a function of the torsional angle. As the torsional angle increases, the band gap shrinks and completely closes at 90°, as shown in **Fig. 3 (d)**. From the molecular orbitals perspective, at 0°, the planar geometry can sustain two fully orthogonal *p*-bands formed by *p<sub>y</sub>* and *p<sub>z</sub>* orbitals, respectively,—the HOMO and LUMO of the molecule (*D*<sub>2h</sub> symmetry). However, when the handles are at 90° (*D*<sub>2d</sub>), the two orbitals become completely equivalent by symmetry and, hence, degenerate. As a result, the energy of the system is increased—**Fig. 3 (e)**. We can estimate this energy change as  $2 \times [E_g/2] = E_g$ , the band gap of the planar molecule, and the resulting potential energy (PE) curve can be approximated by its first Fourier term as  $E(\theta) = \frac{1}{2}(1 - \cos 2\theta)E_g$ . Then, according to Eq. (3), the torsional stiffness is  $H(E_g, L) = 2E_g \times L$ .

Next we examine the behavior of  $E_g$  as a function of  $L$ . Treating carbyne as a 1D potential well of width  $L \equiv Na$ , the HOMO and LUMO energies are  $E_N \propto k_N^2 \propto N^2/L^2$  and  $E_{N+1} \propto k_{N+1}^2 \propto (N+1)^2/L^2$ , and therefore,  $E_g \propto (1+2N)/L^2 \propto 1/L$  for long chains,  $N \gg 1$ . The inverse dependence of the band gap on the length,  $E_g = C/L$ , leads to  $H = 2C = \text{const}$ , *i.e.*, the torsional stiffness of carbyne has a finite constant value.

Both predictions— $E_g \propto 1/L$  and a constant torsional stiffness  $H$ —are confirmed by our DFT calculations, as shown in **Fig. 3 (f)** and **(g)**, respectively. With the =CH<sub>2</sub> termination, the maximum stiffness value we observe is  $H \approx 10.3 \text{ eV}\cdot\text{\AA}/\text{rad}^2$ . This figure is about half the torsional stiffness of dsDNA,<sup>55</sup> which is truly remarkable given carbyne’s one-atom thickness.

Two more interesting aspects of carbyne’s behavior as a torsional spring deserve to be highlighted. First, upon passing 90° twist, the energy evolution is reversed, and the differential stiffness becomes formally negative. This behavior is quite intriguing, since for a normal beam, the energy would increase monotonously during twisting, whereas for this 1-D carbon chain, the torsional energy exhibits a periodic behavior. Second, as is typical for such situations, the frontier orbital degeneracy at 90° can be lifted *via* spin unpairing. Indeed, our calculations show that at near-90° angles, the spin-triplet state is energetically more favorable<sup>30</sup> and, in fact, becomes the local energy minimum (**Fig. 3 (e)**). A separate torsional stiffness can be defined for this minimum,  $H_T = 8.6$  and  $3.7 \text{ eV}\cdot\text{\AA}/\text{rad}^2$  for  $N = 18$  and  $66$  carbyne chains, respectively.

**Equivalent continuum-mechanics model.** To gain further insight and appreciation of the mechanical properties of carbyne, we need to establish the link between the computed atomistic properties and the concepts of continuum elasticity such as the Young’s modulus  $Y$ , the bending stiffness  $K$ , the shear modulus  $G$ . The fully assembled system of equations looks, where all the atomistic quantities (Eqs. 1–

3) are assembled on the left and their counterparts from continuum mechanics, on the right.

$$C = \frac{1}{L^2} \frac{\partial^2 E}{\partial \varepsilon^2} = \frac{\pi r^2 Y}{L}, \quad (4)$$

$$K = \frac{1}{L} \frac{\partial^2 E}{\partial (1/R)^2} = \frac{1}{4} \pi r^4 Y, \quad (5)$$

$$H = L \frac{\partial^2 E}{\partial \theta^2} = 2G\pi r^4. \quad (6)$$

From Eqs. (4) and (5), we can estimate the effective mechanical radius and the Young's modulus of carbyne:  $r = \mathbf{0.386 \text{ \AA}}$  and  $Y = \mathbf{32.71 \text{ TPa}}$ . Knowing the radius, we are now able to compute the shear modulus from (6):  $G = \mathbf{11.8 \text{ TPa}}$ , and thus the effective Poisson's ratio  $n = Y/(2G) - 1$ ,  $n = \mathbf{0.386}$ . Comparing with the hardest natural materials diamond and graphene ( $Y_{\text{diamond}} = 1.22 \text{ TPa}$ ,  $Y_{\text{graphene}} = 1 \text{ TPa}$ ,  $G_{\text{diamond}} = 0.5 \text{ TPa}$ ), we see that carbyne, outperforms them by a factor of about 30 (owing in part to its extremely small mechanical radius). For convenience, the elastic parameters of carbyne are summarized in Table 2.

**Table 2. Summary of mechanical characteristics of carbyne**

<b>Property</b>	<b>Value</b>
thickness $2r$	$0.772 \text{ \AA}$
Young's modulus $Y$	$32.71 \text{ TPa}$
shear modulus $G$	$11.8 \text{ TPa}$
Poisson's ratio $n$	$0.386$
persistence length at 300 K	$14 \text{ nm}$



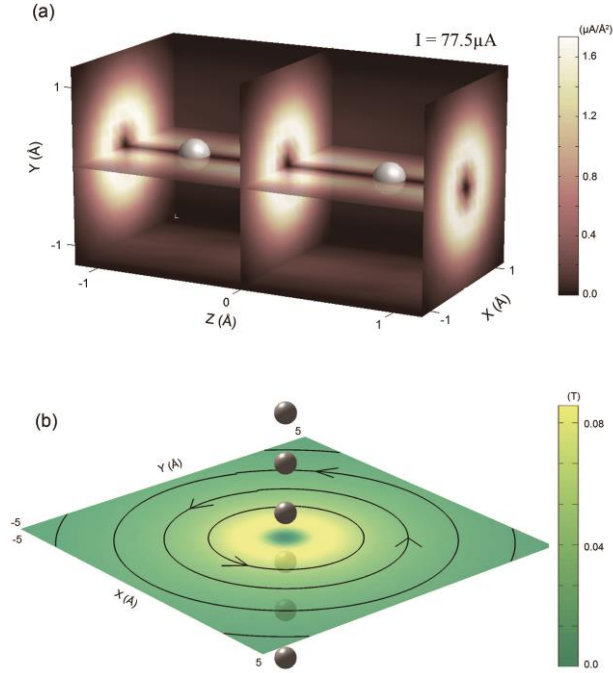


**Figure 4. Carbyne as a conducting cable. (a)** Current density distributions in the axial plane of carbyne and in cross-section. **(b)** The magnetic field induced by the current density of (a). The directions of magnetic vectors correspond to the current flowing from the bottom up.

**Carbyne as a conducting cable.** To investigate the characteristics of carbyne as a conductor, we computed the distribution of electrical current density using the standard real-space nonequilibrium Green's function approach. It gives an explicit form of current density at a given point in space:<sup>57</sup>

$$J(\mathbf{r}) = \frac{1}{2} \sum_{i,j} \int dE \cdot G_{ij}^<(E) \lim_{\mathbf{r}' \rightarrow \mathbf{r}} (\nabla' - \nabla) \phi_i(\mathbf{r}') \phi_j^*(\mathbf{r}), \quad (7)$$

where  $\phi_i$  are the atomic basis functions ( $2s$  and  $2p$ ),  $G^<(E)$  is the matrix correlation function related to the electron density by integration over the energy, and the gradient part corresponds to the probability flux. In addition to integrating the transmission coefficients over the energy range between the two Fermi levels, the total current can also be retrieved by integrating the current density over an arbitrary cross-section of the carbon chain.

**Fig. 4 (a)** shows the calculated current density distribution of a carbon chain. The distribution is axially-symmetric with negligible magnitudes on the axis and a bulge at about  $r = 1 \text{ \AA}$ . This reflects the fact that the  $\sigma$  bonds are localized between atoms and form the skeleton of carbon structures, while the delocalized  $\pi$  bonds normal to the axis support the electronic conductance. By the Biot–Savart–Laplace law, the induced magnetic field can also be determined. As shown in **Fig. 4 (b)**, it exhibits a similar ‘tubular’ distribution pattern.

Similarly to the previous section, it is instructive to estimate what would be the equivalent of carbyne in classical conductors. We may define the effective radius  $r_{eff}$  of the carbyne as the radius of a conducting cylinder that generates an identical inductance to that of carbyne at the same electrical current. The magnetic flux of the

classical conductor per unit length is evaluated by

$$\Phi = \frac{\mu_0}{2\pi} \left( \frac{1}{2} + \ln \frac{R}{r_0} \right) I, \quad (8)$$

where  $R$  is the length of the flux surface,  $r_0$  is the cylinder radius, and  $I$  is the current. With the magnetic field obtained above, the magnetic flux of the carbyne carrying a current  $I$  can be computed if  $R$  is given. We observe a linear dependence between  $\Phi$  and  $I$  of carbyne for various values of  $R = 10\text{--}100 \text{ \AA}$ . Although the slope varies as  $R$  changes, each of them leads to the same  $r_0$  by Eq. (8). Accordingly, the effective radius of carbyne in terms of inductance is found to be  $r_{\text{eff}} = 1.196 \text{ \AA}$ .

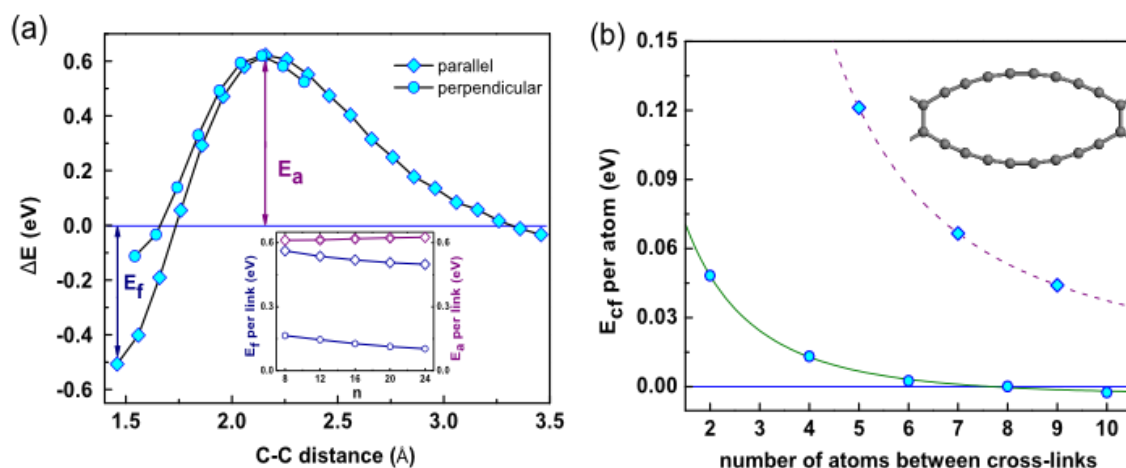


**Figure 5. Cross-linking of carbyne chains.** (a) Potential energy scans showing the barrier of  $\sim 0.6$  eV for finite-length chain crosslinking. (b) Calculations of parallel chain cross-linking patterns suggest a maximum energetically favorable cross-link density of 1 link per 9–11 atoms.  $E = 0$  corresponds to the reference energy level of infinitely isolated carbyne chains.

**Chemical stability of carbyne.** An important concern for any nanoscale material is its stability with respect to dimerization.<sup>58</sup> For carbyne, formation of cross-links between chains is a mechanism of degradation known from experiments,<sup>11</sup> and hence must be studied. **Fig. 5 (a)** shows a relaxed potential energy surface scan using the distance between C atoms in the middle of two carbyne chains as the constraint onto which the reaction coordinate is projected. To avoid introducing bias due to the cumulene/polyne transformation during the cross-link formation, we used two chains with  $2N$  and  $2N + 1$  atoms to simulate the reaction, so that both before and after the reaction there is exactly one chain with an (unfavorable) odd number of atoms in the system. We estimated an activation energy barrier of about  $E_a = 0.6$  eV that is independent of the length of reacting chains (from 8 to 24 atoms) as well as of the dihedral angle formed by the chains. (The overall exothermicity of the reaction showed a weak decrease with the chain length; *i.e.*, shorter chains have a stronger tendency to link.) This barrier suggests the viability of carbyne in condensed phase at room temperature on the order of days.<sup>58</sup>

What will happen if two parallel long carbyne chains are brought into contact? Every cross-link formed will create local curvature, raising the energy of the system. We can estimate the maximum frequency of such cross-links using a simple geometrical model. Assuming all bond angles about a cross-link being  $120^\circ$  and the carbyne curvature between the links remains constant, the length of the arc between two cross-links is  $L = (\pi/3)R$ . The corresponding elastic energy is  $E_{\text{bend}} = KL/2R^2 =$

$K\pi^2/18L = 1.95/L$  eV. This energy cost is offset by the gain from forming the extra bonds between the chains, which is about  $E_f = 0.25$  eV/atom from **Fig. 5 (a)**. Using this value, we arrive at an estimate for  $L \approx 7.8$  Å, or about  $N = 5$  atoms between the cross-links. Compared to the results of DFT calculations presented in **Fig. 5 (b)**, which predict an 8-atom threshold spacing, this is an underestimate that can be straightforwardly attributed to our model's ignoring the  $\pi$ -electron conjugation which is perturbed by the cross-links. Since the energy of conjugation interruption should also scale approximately as  $1/L$ , the general form of  $E_{bend+\pi} = K^*/L$  should still hold. In this case, it is easy to show that the *equilibrium* separation between kinks in an infinite system (one that minimizes the total energy per atom) is exactly twice the *threshold* separation (at which  $E_{bend+\pi} = E_f$ ), and can be estimated from our DFT data as one cross-link per 17 atoms, or 21.8 Å.

Note the oscillating behavior of the DFT data points as the number of atoms between sequential cross-links switches between odd and even. It indicates that the atoms that make the cross-link form a double bond and thus are connected to the chain segments by single bonds, which is only possible to seamlessly integrate into the single–triple alternation pattern of polyynes when the number of atoms in between is even. In fact, odd-number systems are unstable in the sense that if the unit cell is doubled, an  $N = 2M+1$  system tends to reconstruct into a  $\{2P, 2(M-P)\}$  superstructure. An alternative that is favorable for shorter-period systems is to form a pair of adjacent cross-links, resulting in a square  $C_4$  unit (see Supplementary Information for details).

Our finding of a large ( $\sim 2$  nm) equilibrium cross-link spacing explains the experimental observations where single-zigzag-wide graphene nanoribbons show instability and split into pairs of atomic chains.<sup>14</sup> In summary, carbyne chains can be robust against cross-linking at not-too-high temperatures, and mechanical constraints can further prevent them from forming multiple bonds with each other.

## Summary and conclusions

The comprehensive ‘portrait’ of carbyne that we have drawn can be formulated like this. It has an extreme tensile stiffness—stiffer by a factor of two than graphene and carbon nanotubes—and a specific strength surpassing that of any other known material. Its flexibility is between those of typical polymers and double-stranded DNA, with a persistence length of  $\sim 14$  nm. It is equivalent to a continuum-mechanics rod of an extremely small diameter, 0.772 Å, and an enormous nominal Young's modulus of 32.7 TPa. Carbyne can be toggled from the free-rotating to torsionally stiff state by appropriate chemical functionalization ( $=CH_2$ ), in which case its effective shear modulus is about 11.8 TPa, and its formal Poisson's ratio is 0.386. Its band gap increases under tension from 3.2 up to 4.4 eV at a 10% strain, and it is reasonably stable chemically, with an activation barrier of 0.6 eV for cross-linking and an equilibrium link density of one per 2.2 nm (17 atoms) due to  $\pi$ -electron confinement. This combination of unusual mechanical and electronic properties is of great interest for applications in nanomechanical systems, opto-/electromechanical devices, strong and light materials for mechanical applications, or as high-specific-area energy storage matrices.

## Methods

The elastic property calculations and the GW calculations were performed with

VASP<sup>59,60</sup> using the PBE<sup>61,62</sup> generalized-gradient exchange–correlation functional and a 400 eV plane wave cutoff. 12-Å cell spacing was used in the aperiodic directions to eliminate the interaction of periodic images of the system. Structural relaxation was performed until all forces were less than 0.01 eV/Å. Chemical reaction barrier was calculated using the CEP-121G\* basis set<sup>63</sup> in Gaussian 09<sup>64</sup> (spin-unrestricted). The Hamiltonian and overlap matrix elements for quantum transport calculations were computed using SIESTA.<sup>65,66</sup>

## Acknowledgments

We thank M. Hua and Y. Liu for fruitful discussions. The research was supported by the Robert Welch Foundation (C-1590) and the Department of Energy. The computational resources were provided under NSF support.

1. Kroto, H. W.; Heath, J. R.; O'Brien, S. C.; Curl, R. F.; Smalley, R. E. C60: Buckminsterfullerene. *Nature* **1985**, *318*, 162–163.
2. Boehm, H. P.; Clauss, A.; Fischer, G.; Hofmann, U. Thin Carbon Leaves. *Z. Naturforsch.* **1962**, *17b*, 150–153.
3. Novoselov, K. S.; Geim, A. K.; Morozov, S. V.; Jiang, D.; Zhang, Y.; Dubonos, S. V.; Grigorieva, I. V.; Firsov, A. A. Electric Field Effect in Atomically Thin Carbon Films. *Science* **2004**, *306*, 666–669.
4. Bolotin, K.; Sikes, K.; Jiang, Z.; Klima, M.; Fudenberg, G.; Hone, J.; Kim, P.; Stormer, H. Ultrahigh Electron Mobility in Suspended Graphene. *Solid State Commun.* **2008**, *146*, 351–355.
5. Whittaker, A. G. Carbon: A New View of Its High-Temperature Behavior. *Science* **1978**, *200*, 763–764.
6. Goresy, A. E.; Donnay, G. A New Allotropic Form of Carbon from the Ries Crater. *Science* **1968**, *161*, 363–364.
7. Webster, A. Carbyne as a Possible Constituent of the Interstellar Dust. *Mon. Not. R. Astron. Soc.* **1980**, *192*, 7–9.
8. Hayatsu, R.; Scott, R. G.; Studier, M. H.; Lewis, R. S.; Anders, E. Carbynes in Meteorites: Detection, Low-Temperature Origin, and Implications for Interstellar Molecules. *Science* **1980**, *209*, 1515–1518.
9. Jones, R. O.; Seifert, G. Structure and Bonding in Carbon Clusters C<sub>{14}</sub> to C<sub>{24}</sub>: Chains, Rings, Bowls, Plates, and Cages. *Phys. Rev. Lett.* **1997**, *79*, 443–446.
10. Lagow, R. J.; Kampa, J. J.; Wei, H.-C.; Battle, S. L.; Genge, J. W.; Laude, D. A.; Harper, C. J.; Bau, R.; Stevens, R. C.; Haw, J. F.; *et al.* Synthesis of Linear Acetylenic Carbon: The “Sp” Carbon Allotrope. *Science* **1995**, *267*, 362–367.
11. Kavan, L.; Hlavatý, J.; Kastner, J.; Kuzmany, H. Electrochemical Carbyne from Perfluorinated Hydrocarbons: Synthesis and Stability Studied by Raman Scattering. *Carbon* **1995**, *33*, 1321–1329.
12. Casari, C. S.; Bassi, A. Li; Ravagnan, L.; Siviero, F.; Lenardi, C.; Piseri, P.; Bongiorno, G.; Bottani, C. E.; Milani, P. Chemical and Thermal Stability of Carbyne-like Structures in Cluster-assembled Carbon Films. *Phys. Rev. B* **2004**, *69*, 075422.

13. *Polyynes : Synthesis, Properties, and Applications*; Cataldo, F., Ed.; CRC Press: Boca Raton, 2005.
14. Jin, C.; Lan, H.; Peng, L.; Suenaga, K.; Iijima, S. Deriving Carbon Atomic Chains from Graphene. *Phys. Rev. Lett.* **2009**, *102*, 205501.
15. Hobi, E.; Pontes, R. B.; Fazzio, A.; Silva, A. J. R. da Formation of Atomic Carbon Chains from Graphene Nanoribbons. *Phys. Rev. B* **2010**, *81*, 201406.
16. Erdogan, E.; Popov, I.; Rocha, C.; Cuniberti, G.; Roche, S.; Seifert, G. Engineering Carbon Chains from Mechanically Stretched Graphene-based Materials. *Phys. Rev. B* **2011**, *83*, 041401.
17. Yakobson, B. I.; Campbell, M. P.; Brabec, C. J.; Bernholc, J. High Strain Rate Fracture and C-chain Unraveling in Carbon Nanotubes. *Comp. Mater. Sci.* **1997**, *8*, 341–348.
18. Chalifoux, W.; Tykwinski, R. Synthesis of Polyynes to Model the Sp-carbon Allotrope Carbyne. *Nature Chem.* **2010**, *2*, 967–971.
19. Khoo, K. H.; Neaton, J. B.; Son, Y. W.; Cohen, M. L.; Louie, S. G. Negative Differential Resistance in Carbon Atomic Wire–Carbon Nanotube Junctions. *Nano Lett.* **2008**, *8*, 2900–2905.
20. Zanolli, Z.; Onida, G.; Charlier, J.-C. Quantum Spin Transport in Carbon Chains. *ACS Nano* **2010**, *4*, 5174–5180.
21. Zeng, M. G.; Shen, L.; Cai, Y. Q.; Sha, Z. D.; Feng, Y. P. Perfect Spin-filter and Spin-valve in Carbon Atomic Chains. *Appl. Phys. Lett.* **2010**, *96*, 042104–042104–3.
22. Akdim, B.; Pachter, R. Switching Behavior of Carbon Chains Bridging Graphene Nanoribbons: Effects of Uniaxial Strain. *ACS Nano* **2011**, *5*, 1769–1774.
23. Artyukhov, V. I.; Liu, M.; Yakobson, B. I. Mechanically Induced Metal-insulator Transition in Carbyne. *arXiv:1302.7250* **2013**.
24. Sorokin, P. B.; Lee, H.; Antipina, L. Y.; Singh, A. K.; Yakobson, B. I. Calcium-Decorated Carbyne Networks as Hydrogen Storage Media. *Nano Lett.* **2011**, *11*, 2660–2665.
25. Movsisyan, L. D.; Kondratuk, D. V.; Franz, M.; Thompson, A. L.; Tykwinski, R. R.; Anderson, H. L. Synthesis of Polyynes Rotaxanes. *Org. Lett.* **2012**, *14*, 3424–3426.
26. Weisbach, N.; Baranová, Z.; Gauthier, S.; Reibenspies, J. H.; Gladysz, J. A. A New Type of Insulated Molecular Wire: a Rotaxane Derived from a Metal-capped Conjugated Tetrayne. *Chem. Commun.* **2012**, *48*, 7562–7564.
27. Liu, M.; Lee, H.; Yakobson, B. I. Carbynes by the First Principles Computations: an Ultimate 1D-Material. In *ASME 2012 International Mechanical Engineering Congress & Exposition*; Houston, TX, USA, 2012; pp. IMECE2012–89610.
28. Abdurahman, A.; Shukla, A.; Dolg, M. Ab Initio Many-body Calculations on Infinite Carbon and Boron-nitrogen Chains. *Phys. Rev. B* **2002**, *65*, 115106.
29. Tongay, S.; Durgun, E.; Ciraci, S. Atomic Strings of Group IV, III–V, and II–VI Elements. *Appl. Phys. Lett.* **2004**, *85*, 6179–6181.
30. Ravagnan, L.; Manini, N.; Cincuenta, E.; Onida, G.; Sangalli, D.; Motta, C.;

- Devetta, M.; Bordoni, A.; Piseri, P.; Milani, P. Effect of Axial Torsion on Sp Carbon Atomic Wires. *Phys. Rev. Lett.* **2009**, *102*, 245502.
31. Hu, Y. H. Bending Effect of sp-Hybridized Carbon (Carbyne) Chains on Their Structures and Properties. *J. Phys. Chem. C* **2011**, *115*, 1843–1850.
  32. Nair, A. K.; Cranford, S. W.; Buehler, M. J. The Minimal Nanowire: Mechanical Properties of Carbyne. *Europhys. Lett.* **2011**, *95*, 16002.
  33. Castelli, I. E.; Salvestrini, P.; Manini, N. Mechanical Properties of Carbynes Investigated by Ab Initio Total-energy Calculations. *Phys. Rev. B* **2012**, *85*, 214110.
  34. Kertesz, M.; Koller, J.; Azman, A. Ab Initio Hartree–Fock Crystal Orbital Studies. II. Energy Bands of an Infinite Carbon Chain. *J. Chem. Phys.* **1978**, *68*, 2779–2782.
  35. Lee, C.; Wei, X.; Kysar, J. W.; Hone, J. Measurement of the Elastic Properties and Intrinsic Strength of Monolayer Graphene. *Science* **2008**, *321*, 385–388.
  36. Liu, F.; Ming, P.; Li, J. Ab Initio Calculation of Ideal Strength and Phonon Instability of Graphene Under Tension. *Phys. Rev. B* **2007**, *76*, 064120.
  37. Sánchez-Portal, D.; Artacho, E.; Soler, J. M.; Rubio, A.; Ordejón, P. Ab Initio Structural, Elastic, and Vibrational Properties of Carbon Nanotubes. *Phys. Rev. B* **1999**, *59*, 12678–12688.
  38. Spear, K. E.; Dismukes, J. P. *Synthetic Diamond: Emerging CVD Science and Technology*; Electrochemical Society; Wiley: New York, 1994.
  39. Dumitrica, T.; Hua, M.; Yakobson, B. I. Symmetry-, Time-, and Temperature-dependent Strength of Carbon Nanotubes. *Proc. Natl. Acad. Sci. U.S.A.* **2006**, *103*, 6105–6109.
  40. Ogata, S.; Shibutani, Y. Ideal Tensile Strength and Band Gap of Single-walled Carbon Nanotubes. *Phys. Rev. B* **2003**, *68*, 165409.
  41. Chang, C.-C.; Hsu, I.-K.; Aykol, M.; Hung, W.-H.; Chen, C.-C.; Cronin, S. B. A New Lower Limit for the Ultimate Breaking Strain of Carbon Nanotubes. *ACS Nano* **2010**, *4*, 5095–5100.
  42. Telling, R. H.; Pickard, C. J.; Payne, M. C.; Field, J. E. Theoretical Strength and Cleavage of Diamond. *Phys. Rev. Lett.* **2000**, *84*, 5160–5163.
  43. Hybertsen, M. S.; Louie, S. G. Electron Correlation in Semiconductors and Insulators: Band Gaps and Quasiparticle Energies. *Phys. Rev. B* **1986**, *34*, 5390–5413.
  44. Spataru, C. D.; Ismail-Beigi, S.; Benedict, L. X.; Louie, S. G. Excitonic Effects and Optical Spectra of Single-Walled Carbon Nanotubes. *Phys. Rev. Lett.* **2004**, *92*, 077402.
  45. Yang, L.; Park, C.-H.; Son, Y.-W.; Cohen, M. L.; Louie, S. G. Quasiparticle Energies and Band Gaps in Graphene Nanoribbons. *Phys. Rev. Lett.* **2007**, *99*, 186801.
  46. Cretu, O.; Botello-Mendez, A. R.; Janowska, I.; Pham-Huu, C.; Charlier, J.-C.; Banhart, F. Electrical Transport Measured in Atomic Carbon Chains. *Nano Lett.* **2013**.

47. Bylaska, E. J.; Weare, J. H.; Kawai, R. Development of Bond-length Alternation in Very Large Carbon Rings: LDA Pseudopotential Results. *Phys. Rev. B* **1998**, *58*, R7488–R7491.
48. Torelli, T.; Mitas, L. Electron Correlation in C<sub>{4N+2}</sub> Carbon Rings: Aromatic Versus Dimerized Structures. *Phys. Rev. Lett.* **2000**, *85*, 1702–1705.
49. Saito, M.; Okamoto, Y. Second-order Jahn-Teller Effect on Carbon 4N+2 Member Ring Clusters. *Phys. Rev. B* **1999**, *60*, 8939–8942.
50. Ganster, J.; Fink, H.-P.; Zenke, I. Chain Conformation of Polyacrylonitrile: a Comparison of Model Scattering and Radial Distribution Functions with Experimental Wide-angle X-ray Scattering Results. *Polymer* **1991**, *32*, 1566–1573.
51. Severin, M.; Inganäs, O. Global Conformation and Order Parameters of Doped Polyacetylene at Finite Temperatures. *Europhys. Lett.* **1994**, *25*, 347–352.
52. Smith, S. B.; Cui, Y.; Bustamante, C. Overstretching B-DNA: The Elastic Response of Individual Double-Stranded and Single-Stranded DNA Molecules. *Science* **1996**, *271*, 795–799.
53. Tinland, B.; Pluen, A.; Sturm, J.; Weill, G. Persistence Length of Single-Stranded DNA. *Macromolecules* **1997**, *30*, 5763–5765.
54. Gettinger, C. L.; Heeger, A. J.; Pine, D. J.; Cao, Y. Solution Characterization of Surfactant Solubilized Polyaniline. *Synt. Met.* **1995**, *74*, 81–88.
55. Hagerman, P. J. Flexibility of DNA. *Annu. Rev. Biophys. Biophys. Chem.* **1988**, *17*, 265–286.
56. Bets, K. V.; Yakobson, B. I. Spontaneous Twist and Intrinsic Instabilities of Pristine Graphene Nanoribbons. *Nano Res.* **2009**, *2*, 161–166.
57. Xue, Y.; Datta, S.; Ratner, M. A. First-principles Based Matrix Green's Function Approach to Molecular Electronic Devices: General Formalism. *Chem. Phys.* **2002**, *281*, 151–170.
58. Hoffmann, R. Small but Strong Lessons from Chemistry for Nanoscience. *Angew. Chem. Int. Ed.* **2013**, *52*, 93–103.
59. Kresse, G.; Hafner, J. Ab Initio Molecular Dynamics for Liquid Metals. *Phys. Rev. B* **1993**, *47*, 558–561.
60. Kresse, G.; Furthmüller, J. Efficient Iterative Schemes for Ab Initio Total-energy Calculations Using a Plane-wave Basis Set. *Phys. Rev. B* **1996**, *54*, 11169–11186.
61. Perdew, J. P.; Burke, K.; Ernzerhof, M. Generalized Gradient Approximation Made Simple. *Phys. Rev. Lett.* **1996**, *77*, 3865–3868.
62. Perdew, J. P.; Burke, K.; Ernzerhof, M. Generalized Gradient Approximation Made Simple [Phys. Rev. Lett. 77, 3865 (1996)]. *Phys. Rev. Lett.* **1997**, *78*, 1396.
63. Stevens, W. J.; Basch, H.; Krauss, M. Compact Effective Potentials and Efficient Shared-exponent Basis Sets for the First- and Second-row Atoms. *J. Chem. Phys.* **1984**, *81*, 6026–6033.
64. Frisch, M. J.; Trucks, G. W.; Schlegel, H. B.; Scuseria, G. E.; Robb, M. A.; Cheeseman, J. R.; Scalmani, G.; Barone, V.; Mennucci, B.; Petersson, G. A.; *et al.* *Gaussian 09 Revision A.1.*

65. Soler, J. M.; Artacho, E.; Gale, J. D.; García, A.; Junquera, J.; Ordejón, P.; Sánchez-Portal, D. The SIESTA Method for Ab Initio order-N Materials Simulation. *Journal of Physics: Condensed Matter* **2002**, *14*, 2745–2779.
66. Artacho, E.; Anglada, E.; Diéguez, O.; Gale, J. D.; García, A.; Junquera, J.; Martin, R. M.; Ordejón, P.; Pruneda, J. M.; Sánchez-Portal, D.; *et al.* The SIESTA Method; Developments and Applicability. *Journal of Physics: Condensed Matter* **2008**, *20*, 064208.



# Supplementary Information

**Determination of the tensile strength of carbyne.** We used two methods to estimate the strength. Figure S1 (a–c) illustrates the evolution of phonon dispersions of carbyne (calculated with the finite-displacement method using the *PHON* software with a 12-atom supercell). At a 19% strain (c), imaginary frequencies appear (shown as negative), which marks the onset of the phonon instability corresponding to the upper limit of ideal strength of a material. (At the same time, the force vs. strain plot starts going down—not shown.)

The other approach is to treat bond breaking as an activated process. In the standard Arrhenius form, the bond-breaking rate is  $R = A \exp[-E_a(\varepsilon) / kT]$  where  $E_a$  is the activation energy and  $A$  is the “attempt frequency” prefactor.  $A$  can be estimated based on the bond stretching phonon frequency, e.g., in Figure S1 (a), as  $4 \times 10^{13} \text{ s}^{-1}$ .  $E_a$  is computed using a supercell setup (24 atoms) where one of the bonds is incrementally stretched by  $\Delta d$  relaxing the positions of all other atoms to get a potential energy profile, as shown in Figure S1 (d). The resulting exponential decrease of  $E_a$  with strain is illustrated in Figure S1 (e). As a useful point of reference,  $E_a = 1 \text{ eV}$  corresponds to a lifetime of about  $R^{-1} \approx 1 \text{ day}$  at room temperature. This occurs at a strain of 9%, corresponding to a force of 9.2–9.3 nN (inset). It should be noted that for a chain with  $N$  bonds, the prefactor is multiplied by  $N$ ; another way to view this is to replace  $E_a$  with the free energy barrier  $\Delta G^* = E_a - kT \log N$ . We see that this addition results in only a logarithmic correction in  $E_a$ , and since  $E_a$  is exponential in strain, the breaking strain and force change negligibly slowly with  $N$  (as  $\sim \log[\log N]$ ).

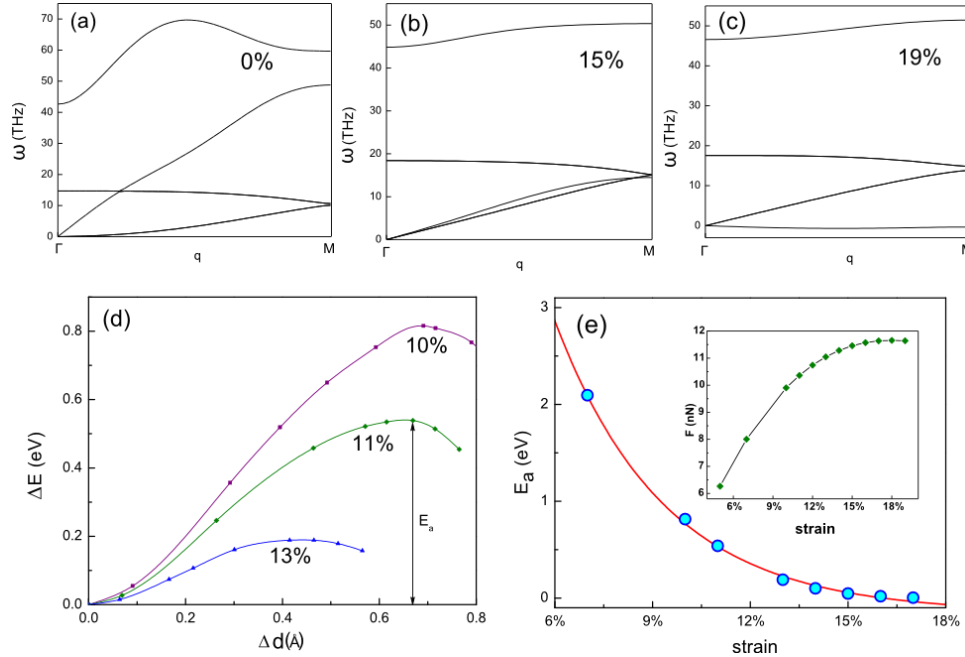


**Figure S1.** Determination of the tensile strength of carbyne. **(a–c)** Phonon dispersion plots at 0, 15%, and 19% strain showing phonon instability (imaginary frequencies in **(c)**). **(d)** Bond breaking reaction profiles and **(e)** activation energy as a function of strain. The **inset** in (e) shows the force vs. strain curve.

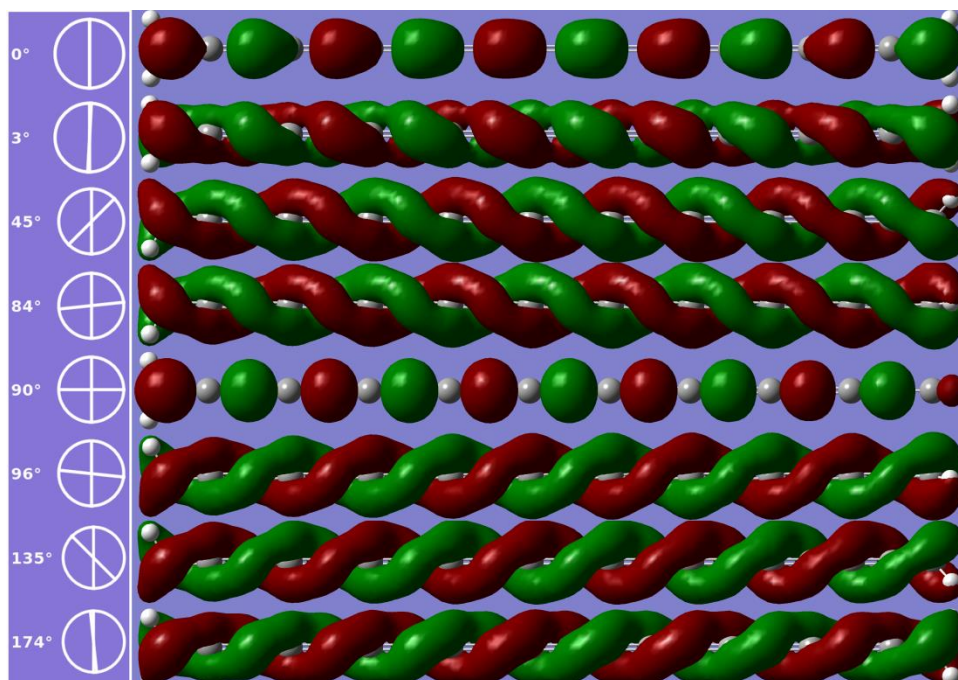


**Figure S2.** The evolution of highest occupied molecular orbital (HOMO) in an 18-atom carbyne chain with  $=\text{CH}_2$  end-group handles under torsion. Green and red represent the opposite signs of the  $\pi$  orbital.

**Ambiguity of length in torsional stiffness definition.** The torsional stiffness of a beam is defined by the product of its length  $L$  and the second derivative of energy in the twist angle. However, for carbyne chains with, e.g.,  $=\text{CH}_2$  terminating groups it is unclear whether the C atom of the endgroup should be considered part of the “beam” or not. More generally, we can declare that  $L = L' + \Delta$ , where  $L'$  is the distance between the outermost C atoms and  $\Delta$  is a small adjustable fitting parameter. Fitting  $H = H_0 + h/(L' + \Delta)$  yields  $H_0 = 10.52$  with a less than 2% deviation from the result reported in the main text.

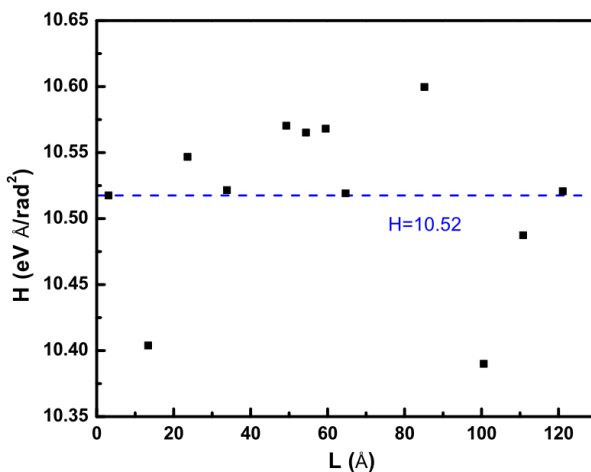


**Figure S3.** Simultaneous fitting of  $H$  and  $L$ .

**Reconstructions of odd-spaced cross-linked systems.** Figure 5 of the main text shows that the cross-linked systems with odd numbers of atoms between the cross-links are unstable (due to bond-order alternation issues). There are several possible relaxation mechanisms in such systems, with their energies illustrated in Figure S4. The simplest mechanism is the formation of an extra cross-link when the initial odd  $N = 4P + 1$  can be split in two even-spaced intervals of  $2(P - Q)$  and  $2(P + Q)$ . This type of transition is illustrated by blue hollow circles in Figure S4, where the  $N = 5$  system is converted into  $N = 2$ , and  $N = 7$  into alternating  $N = 2$  and  $N = 4$  fragments. As it turns out, in both cases it is energetically more favorable to form the second cross-link next to the existing one, creating a square  $C_4$  unit, and for the  $N = 3$  system this happens to occur spontaneously (yellow triangles). Finally, it is possible to form 2x superstructures by shifting every other cross-link one atom to the side, turning the 5555... system into 4646... and similarly for other even  $N$ . This process is shown by solid blue circles and gray arrows. Figure S4 (b), (c), (d) shows three different structures for  $N = 7$  atoms in the periodic cell, corresponding to the diamond, hollow circle and triangle in (a).

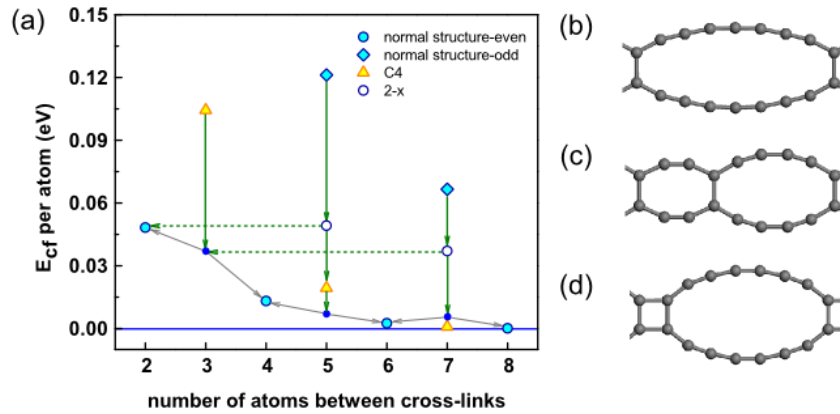


**Figure S4.** Reconstructions of unstable cross-linked structures.